JOURNAL OF SPACECRAFT AND ROCKETS
Vol. 35, No. 3, May–June 1998

Shuttle Orbiter Experimental Boundary-Layer Transition Results with Isolated Roughness

Scott A. Berry*
NASA Langley Research Center, Hampton, Virginia 23681
Stanley A. Bouslog†
B. F. Goodrich Aerospace, Chula Vista, California 91910
Gregory J. Brauckmann*
NASA Langley Research Center, Hampton, Virginia 23681
and
Jose M. Caram‡
NASA Johnson Space Flight Center, Houston, Texas 77058

The effect of isolated roughness on the windward surface boundary layer of the Shuttle Orbiter has been experimentally examined in the NASA Langley Research Center 20-Inch Mach 6 Tunnel. The size and location of isolated roughness elements (intended to simulate raised or misaligned Shuttle Orbiter Thermal Protection System tiles and protruding gap filler material) were varied to systematically examine the response of the boundary layer. Global heat transfer images of the windward surface of a 0.75%-scale Orbiter at an angle of attack of 40 deg were obtained over a range of Reynolds numbers using phosphor thermography and were used to infer the status of the boundary layer. Computational predictions were performed to provide both laminar and turbulent heating levels for comparison to the experimental data and to provide flowfield parameters used for investigating boundary-layer transition correlations. A variety of roughness heights and locations along the windward centerline were used. The roughness-transition correlation, using the predicted edge parameters Re_θ/M_e and k/δ, was well behaved. The off-centerline results illustrate the potential for an asymmetric transition pattern to be isolated to one side of the vehicle, thereby causing the increased yawing moments experienced in flight.

Nomenclature

H	= enthalpy, Btu/lbm
h	= heat transfer coefficient, lbm/ft^2-s, $=q/(H_{aw} - H_w)$, where $H_{aw} = H_{t2}$
h_{F-R}	= reference coefficient using Fay–Ridell calculation to stagnation point of a sphere
k	= roughness element height, in.
L	= reference length of model, 10.25 in.
M	= Mach number
p	= pressure, psi
q	= heat transfer rate, Btu/ft^2-s
Re	= unit Reynolds number, 1/ft
Re_θ	= momentum thickness Reynolds number
T	= temperature, °R
x	= longitudinal distance from the nose, in.
α	= model angle of attack, deg
δ	= boundary-layer thickness, in.
ϕ_{lat}	= disturbance lateral spreading angle, deg

Subscripts

aw	= adiabatic wall
e	= local edge condition
eff	= effective
inc	= incipient
$t1$	= reservoir conditions
$t2$	= stagnation conditions behind normal shock
w	= model surface
∞	= freestream static conditions

Received Feb. 13, 1997; revision received July 22, 1997; accepted for publication July 29, 1997.

*Aerospace Technologist, Aerothermodynamics Branch, Aero- and Gas-Dynamics Division.
†Group Engineer. Associate Fellow AIAA.
‡Aerospace Engineer, Aerospace Flight Mechanics Division. Senior Member AIAA.

Introduction

THE fleet of Space Shuttle Orbiters have flown over 75 missions, each concluding with a hypersonic re-entry through the Earth's atmosphere. During the hypersonic re-entry, the boundary layer on the windward surface of the Orbiter transitions from laminar to turbulent flow. The time at which this transition takes place during the re-entry has a significant effect on the total heat load absorbed by the Orbiter. Nominally, windward surface transition occurs approximately 1200 s from the entry interface altitude of 400,000 ft (which approximately corresponds to a Mach number of 8). However, during several missions, transition has occurred significantly earlier, with STS-28 and STS-73 having the earliest transition times of 900 and 890 s, respectively (approximately Mach 17). For both of these flights, the early transition has been attributed to gap filler material protruding from between the thermal protection system (TPS) tiles into the boundary-layer flow of the vehicle. These protruding gap fillers represent discrete roughness elements that can trip the boundary layer. Furthermore, for several missions, yawing moments on the vehicle during re-entry have been attributed to asymmetric transition on the windward surface and have required significant reaction control system propellant to correct. Again, it has been hypothesized that a protuberance, such as a gap filler, on one side of the vehicle has tripped the boundary layer, thereby resulting in a side-to-side difference in skin friction.

To investigate these anomalies, two wind-tunnel tests were planned and conducted to obtain a better understanding of boundary-layer transition on the Orbiter windward surface induced by isolated roughness elements. The first test, described in Ref. 1, was conducted with a 1.75%-scale Orbiter model in the Arnold Engineering Development Center (AEDC) Tunnel B. The second test was conducted with a 0.75%-scale Orbiter model in the NASA Langley Research Center (LaRC) 20-Inch Mach 6 Tunnel and is described and discussed in this paper. The AEDC study used existing model

hardware and an established testing technique (coaxial thermocouples) to provide high-quality data that could be compared directly to similar data obtained earlier in the Orbiter program. The LaRC study was designed specifically to take advantage of the phosphor thermography technique to provide global heating information and better spatial resolution of the disturbances behind the roughness elements.

The extensive Orbiter flight database provides an opportunity to validate and calibrate ground-based boundary-layer transition experiments and thus improve hypersonic transition prediction methodology. Future space transportation systems will have to implement similar procedures and test techniques in ground-based facilities to predict the boundary-layer status during the hypersonic re-entry. Accurate prediction of the time during re-entry when the boundary-layer transition from laminar to turbulent flow occurs has a direct impact on the design of the TPS and thus the weight and cost of the vehicle.

Experimental Methods

Facility

The present experiment was conducted in the LaRC 20-Inch Mach 6 Tunnel. A detailed description of this facility, along with performance characteristics, is presented in Ref. 2. It is a hypersonic blow-down facility that uses heated, dried, and filtered air as the test gas. Typical operating conditions for the tunnel are stagnation pressures ranging from 30 to 500 psia, stagnation temperatures from 760 to 1000°R, and freestream unit Reynolds numbers from 0.5×10^6 to 8×10^6/ft. A two-dimensional, contoured nozzle is used to provide nominal freestream Mach numbers from 5.8 to 6.1. The test section is 20.5 × 20 in.; the nozzle throat is 0.399 × 20.5 in. A bottom-mounted model injection system can insert models from a sheltered position to the tunnel centerline in less than 0.5 s. Run times up to 15 min are possible with this facility, although for the current heat transfer tests, run times were only a few seconds.

Test Technique

The rapid advances in image processing technology that have occurred in recent years have made digital optical measurement techniques practical in the wind tunnel. One such optical acquisition method is two-color, relative-intensity phosphor thermography, which is being applied to aerothermodynamic testing in the NASA LaRC hypersonic wind tunnels.[3–6] With this technique, ceramic wind-tunnel models are fabricated and coated with phosphors that fluoresce in two regions of the visible spectrum when illuminated with uv light. The fluorescence intensity is dependent on the amount of incident uv light and the local surface temperature of the phosphors. By acquiring fluorescence intensity images, with a color video camera, of an illuminated phosphor model exposed to flow in a wind tunnel, surface temperature mappings can be calculated on the portions of the model that are in the field of view of the camera. A temperature calibration of the system conducted prior to the study provides the lookup tables that convert the ratio of the green and the red intensity images to global temperature mappings. By use of temperature images acquired at different times in a wind-tunnel run, global heat transfer images are computed assuming one-dimensional heat conduction. The acquisition system for the phosphor thermography technique is video based; thus the images are acquired at 30 frames/s. At this framing rate, the phosphor response can be considered to be instantaneous. Typically, only a few images are saved and analyzed because the memory-storage requirements per image are quite high. The current results are analyzed at 2.5 s after the start of injection. This time was selected for this facility to allow sufficient temperature increase on the model. (The calculated thermal penetration depth is less than half the ceramic shell thickness of 0.3 in.) The primary advantage of this technique is the global resolution of the quantitative heat transfer data. Such data can be used to identify the heating footprint of complex, three-dimensional flow phenomena, e.g., transition fronts, turbulent wedges, boundary-layer vortices, that are extremely difficult to resolve by discrete measurement techniques. Phosphor thermography now is used routinely in NASA LaRC's hypersonic facilities because quantitative global heating information is provided by models that can be fabricated much quicker and cheaper than other "more conventional" techniques.

Models

To obtain accurate heat transfer data using the one-dimensional heat conduction equation, models need to be made of a material with low thermal diffusivity and well-defined, uniform, isotropic thermal properties. Also, the models must be durable for repeated use in the wind tunnel and not deform when thermally cycled. To meet these requirements, a unique, silica ceramic investment slip casting method has been developed and patented.[7] Utilizing this method, several ceramic 0.75%-scale Orbiter models were fabricated with a body-flap deflection of 0 deg. For this scale, the reference dimension, typically taken from the nose to the body-flap hinge line, was 9.68-in. A hydraulically setting magnesia ceramic was used to backfill the ceramic shell, thus providing strength and support to the sting structure. The models then were coated with a mixture of phosphors suspended in a silica-based colloidal binder. This coating consisted of a 5:1 mixture of lanthanum oxysulfide (La_2O_2S) doped with trivalent europium and zinc cadmium sulfide (ZnCdS) doped with silver and nickel in a proprietary ratio. The coatings typically do not require refurbishment between runs in the wind tunnel and have been measured to be approximately 0.001 in. thick. The final step in the fabrication process is to apply fiducial marks along the body to assist in accurately determining spatial locations. The fiducial marks for these models correspond to the roughness-element locations and are shown in Fig. 1. These locations were chosen in

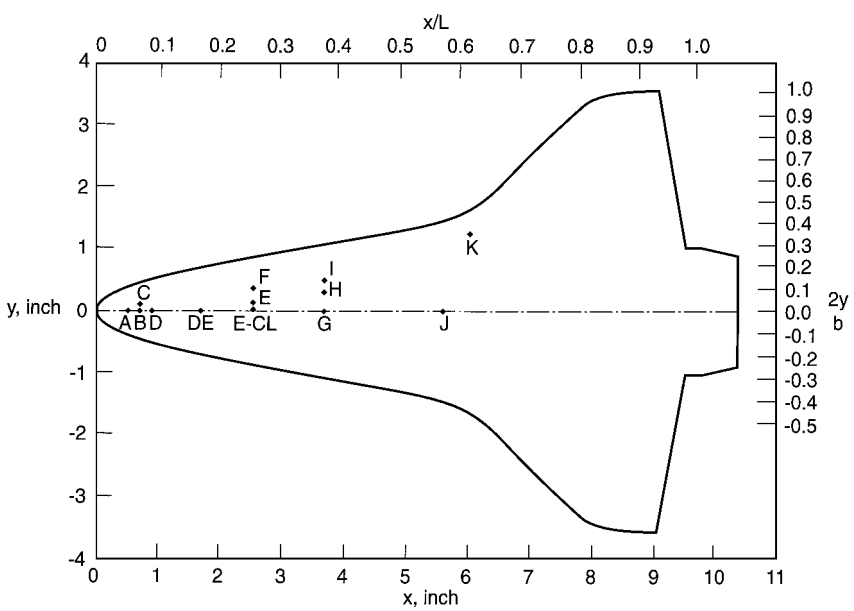

Fig. 1 Sketch of LaRC Orbiter model windward surface showing roughness-element locations.

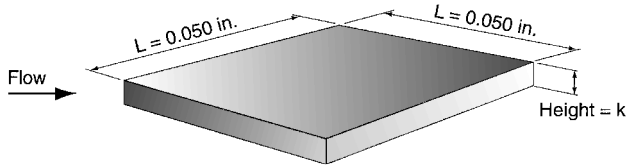

Fig. 2 Sketch of roughness element showing size and orientation; k = 0.0025, 0.0050, 0.0075, and 0.0100 in.

coordination with the AEDC study,[1] which had several roughness locations along the centerline (points A, B, D, G, and J) and several off centerline but on or near the attachment line (points C, E, F, H, I, and K). Locations A, B, C, and D were chosen because of their proximity to the subsonic region near the nose. Two additional roughness locations were added along the centerline (points DE and E-CL) for the present study.

The roughness elements used in this study were fabricated to simulate a raised TPS tile and were cut from 0.0025-in.-thick Kapton® tape. Raised shuttle tiles were modeled, as opposed to the protruding gap fillers for the AEDC study, because on the scale of the present study the protrusions would have been unmanageably small. The nominal 6-in.-square, full-scale shuttle tile scales down to approximately 0.050 in. on a side, which was more manageable. Variations on the roughness heights k were obtained by stacking multiple layers of Kapton tape (k = 0.0025, 0.0050, 0.0075, and 0.0100 in.). Roughness elements fabricated from Kapton tape were applied easily to the various locations of interest on the model without adversely affecting the phosphor coating. Kapton tape was chosen through a trial-and-error process based on the ease of fabrication and application of the roughness elements, as well as the robustness of the material and the adhesive to heat and shear stress. The simulated tile roughness elements were placed directly over the various fiducial marks, which were located previously on the model. A sketch of a typical trip showing dimensions and orientation is presented in Fig. 2.

Test Conditions

The LaRC 20-Inch Mach 6 Tunnel provides a freestream unit Reynolds number variation of 0.5×10^6 to 8.0×10^6/ft. For a 0.75%-scale model, this range corresponds to a length Reynolds number of approximately 0.41×10^6 to 6.7×10^6, which is on the order of the flight-length Reynolds number at the time of transition, which can vary between 2.5×10^6 and 12×10^6 (Ref. 8). With the roughness element firmly applied to the location of interest, the tunnel stagnation pressure and temperature were varied over a series of runs to determine the maximum Reynolds number that still maintained laminar flow (incipient value), the Reynolds number where significant nonlaminar flow first appears downstream of the roughness element (critical), and finally, the minimum Reynolds number where the transition front is fixed at the roughness element (effective value). A more detailed discussion about incipient, critical, and effective Reynolds numbers can be found in several references by Bertin and, in particular, in Ref. 1. The model angle of attack was 40 deg, and the sideslip was maintained at zero for all of the runs presented herein. Flow conditions, including run-to-run repeatability, can be found in Table 1 of Ref. 9.

Data Reduction and Uncertainty

To analyze the large amount of data associated with phosphor thermography, a workstation-based image processing package called IHEAT has been developed by Ron Merski of NASA LaRC. Written in a user-friendly windowing format, IHEAT consists of six programs to handle system calibrations along with data reduction, editing, and viewing. Using IHEAT, data can be reduced to heat transfer images immediately after a run. An automated routine also extracts the heating distribution data along lines of interest, such as centerline and axial cuts. The heating rates are calculated from the global surface temperature measurements using one-dimensional, semi-infinite, solid heat-conduction equations, as discussed in detail in Refs. 4 and 5. On the basis of considerations presented in Ref. 5, phosphor system measurement error is believed to be better than ±8%, with the overall experimental uncertainty ±15%. Heating distributions are presented in terms of the ratio of heat transfer coefficients h/h_{F-R}, where h_{F-R} corresponds to the stagnation-point heating to a sphere[10] with radius 0.09 in. (a 1-ft-radius sphere scaled to the model size). Repeatability of the normalized heat transfer distributions generally was better than ±4%.

Prediction Methods

Computations of surface heating for comparison with the current data set, as well as flowfield parameters used for investigating boundary-layer transition correlations, were performed utilizing a two-layer approach. The two-layer approach was a three-step process. First, an inviscid flowfield about the Orbiter configuration was computed. Second, using the inviscid flowfield as input, a streamline tracing code was used to define the pressure distributions, streamline spreading metrics, and the local boundary-layer edge entropy along the inviscid streamline. Finally, a boundary-layer code was used to compute the surface heating rates and the boundary-layer parameters. The IEC3D inviscid flowfield solver[11] was used to compute the inviscid flowfield for the Orbiter at $\alpha = 40$ deg. The streamline code[12] was used to generate the pressure, the metric, and the edge entropy distributions along inviscid streamlines. The Boundary Layer Integral Matrix Procedure (BLIMP) code[13] was used to compute the surface heating rates and the boundary-layer parameters using perfect-gas assumptions and a fixed wall temperature of 540°R.

Figure 3a presents the laminar boundary-layer thickness on the centerline of the Orbiter model for several wind-tunnel freestream Reynolds numbers. Because roughness elements of 0.0025 to 0.0100 in. were used in this test, the roughness elements never protruded outside of the boundary layer. For most runs, transition occurred

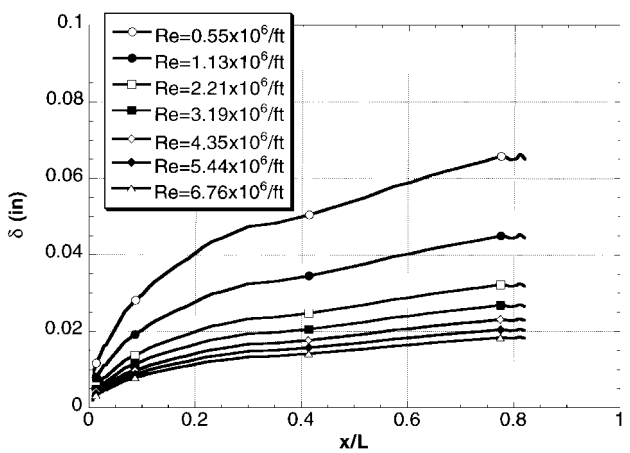

a) Laminar boundary-layer thickness

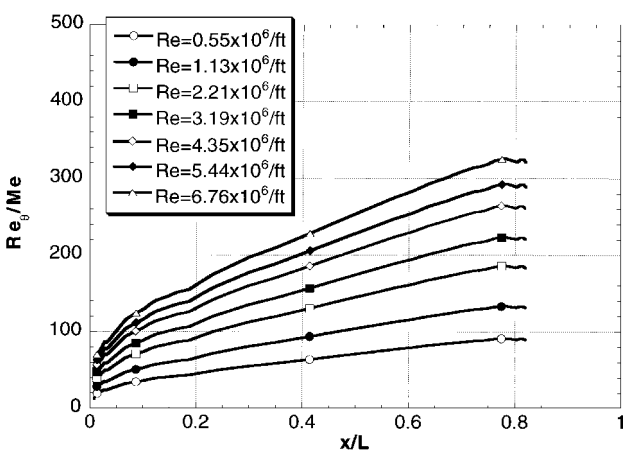

b) Momentum thickness Reynolds number divided by local edge Mach number

Fig. 3 BLIMP predictions along Orbiter model centerline for a range of freestream unit Reynolds numbers (M_∞ = 6, α = 40 deg).

with the roughness elements protruding into the bottom one-third of the boundary layer.

Figure 3b presents the centerline predictions of the transition parameter Re_θ/M_e (the momentum thickness Reynolds number divided by the local edge Mach number) of the Orbiter model for a range of freestream unit Reynolds numbers. This parameter, along with the boundary-layer thickness and the experimental transition results, is used to correlate the data. A more in-depth examination of different correlations using the data set presented here, data from the AEDC study,[1] and flight data has been published in a companion paper.[14]

Discussion of Results

Baseline Results

The gradual onset of transition with increasing Reynolds number for the baseline smooth model can be seen in the heat transfer images presented in Fig. 4. At the lower Reynolds number of

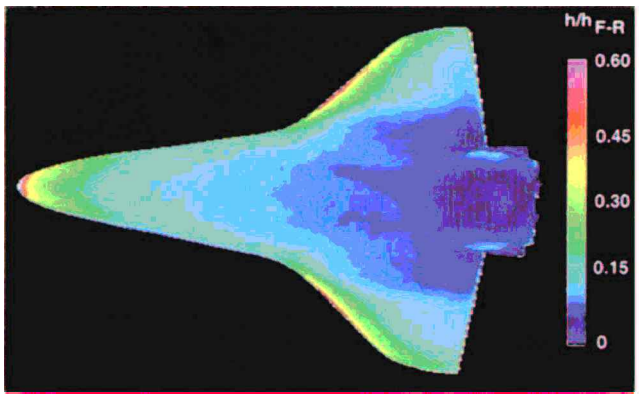

a) $Re_\infty = 2.2 \times 10^6$/ft

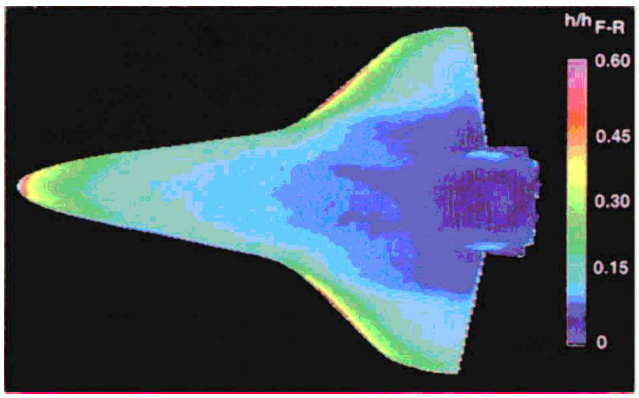

b) $Re_\infty = 4.4 \times 10^6$/ft

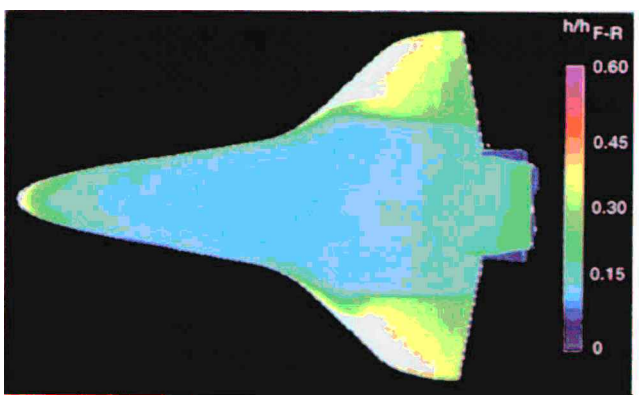

c) $Re_\infty = 6.6 \times 10^6$/ft

Fig. 4 Effect of freestream unit Reynolds number on smooth body transition ($M_\infty = 6$, $\alpha = 40$ deg).

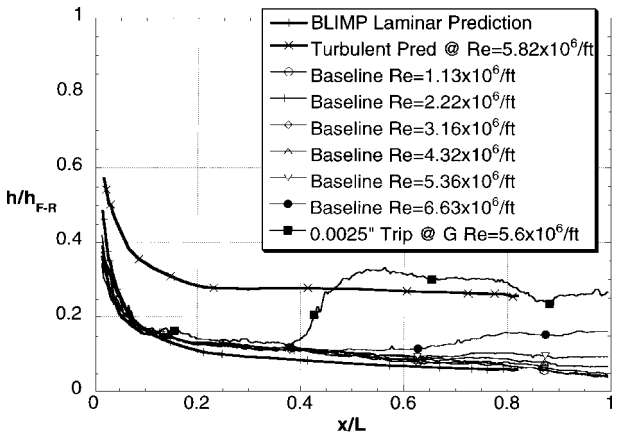

Fig. 5 Centerline heating comparison between measured and predicted results for smooth baseline over a range of Re_∞ and a sample trip case.

2.2×10^6/ft, the windward surface is fully laminar (Fig. 4a); at a freestream Reynolds number of 4.4×10^6/ft (Fig. 4b) transition has begun to appear on the wings but the centerline remains laminar; finally, at the highest Reynolds number of 6.6×10^6/ft (Fig. 4c), the wing appears to be turbulent but transition has just started to appear along the windward centerline. Based on the results presented in Fig. 3b, the onset of transition at $Re = 6.6 \times 10^6$/ft corresponds to a smooth model Re_θ/M_e of approximately 300 at $x/L = 0.6$. The 20-Inch Mach 6 Tunnel is considered a conventional facility in regard to freestream disturbance levels; this tunnel was built long before the quiet-tunnel technology of the 1980s became available. Thus, the freestream disturbances would be expected to influence the smooth-model transition data. In fact, Fig. 12 of Ref. 14 provides a comparison of the present smooth-model data to similar data from AEDC Tunnel B and flight and clearly indicates the effect of tunnel noise on transition data (with the flight value of Re_θ/M_e at transition being the highest and the results from AEDC being the lowest). However, because roughness-induced transition is a known bypass of the linear growth of boundary-layer disturbances, tunnel noise would not be expected to have a first-order impact on the examination of roughness-induced boundary-layer transition.

Figure 5 presents a comparison along the centerline between predicted and measured distributions of the heat transfer coefficient referenced to the Fay–Ridell stagnation-point value. The predictions include both a laminar and a turbulent heating distribution. The experimental data are for a range of freestream unit Reynolds numbers and include the baseline smooth data, as well as data of a sample tripped case. The measured and predicted laminar distributions were observed to be independent of Reynolds number, whereas the turbulent distributions exhibit a slight dependence on Reynolds number. Measured and predicted turbulent results are shown for a freestream unit Reynolds number of 5.8×10^6/ft. The tripped case is shown for comparison with the predicted turbulent heating distribution and reveals that turbulent heating levels are quickly reached just after the trip location of $x/L = 0.375$. Both the laminar and turbulent heating predictions are approximately 20% lower than measured, which is just outside the bounds of the experimental uncertainty. Although the reasons for this underprediction are not known, the effect on the transition correlation parameters that are based on edge conditions (such as those used herein) should be relatively small. For instance, a 30% shift in heating rate produced by an adjustment to the wall temperature resulted in only a 1–2% change in both Re_θ/M_e and δ.

Sample Roughness Results

A significant number of runs were obtained in the 20-Inch Mach 6 Tunnel to define a shuttle-derived, roughness-induced transition correlation. Most of the data were obtained for trip locations along the centerline of the model. It is beyond the scope of this paper to show all data that were obtained; therefore, a few sample cases have been selected to provide trends. Only the centerline results are included in the final correlation plot.

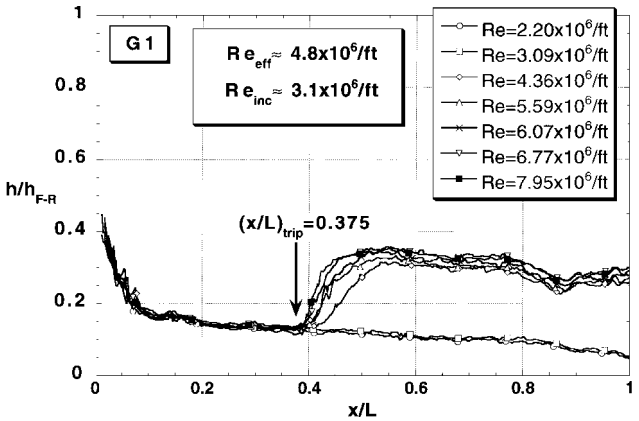

a) 0.0025-in. roughness element

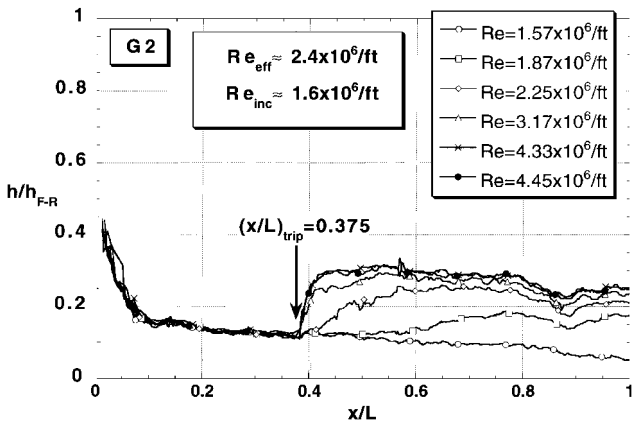

b) 0.0050-in. roughness element

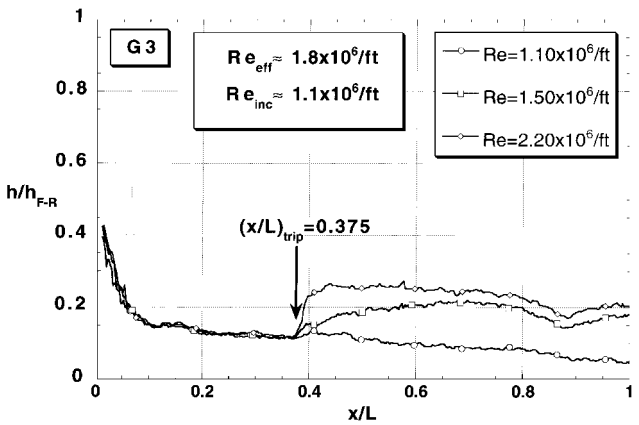

c) 0.0075-in. roughness element

Fig. 6 Centerline heating comparison for a range of trip heights and Re_∞ at location G ($M_\infty = 6$, $\alpha = 40$ deg).

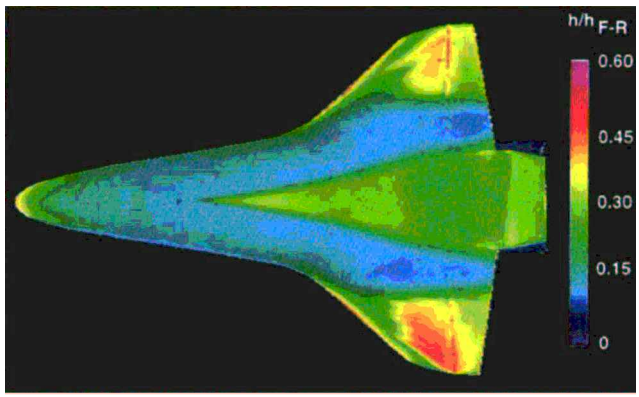

0.0025-in. roughness element and $Re_\infty = 5.6 \times 10^6$/ft

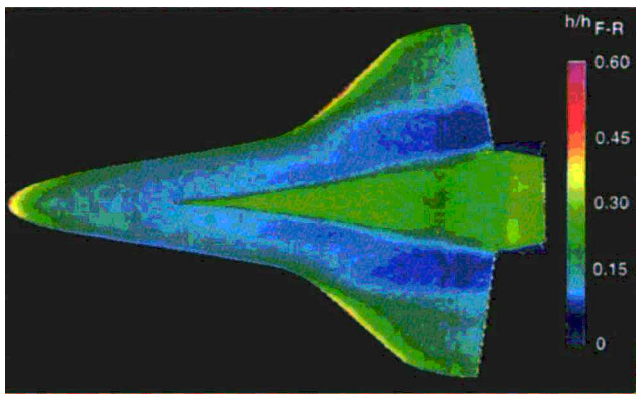

0.0050-in. roughness element and $Re_\infty = 3.2 \times 10^6$/ft

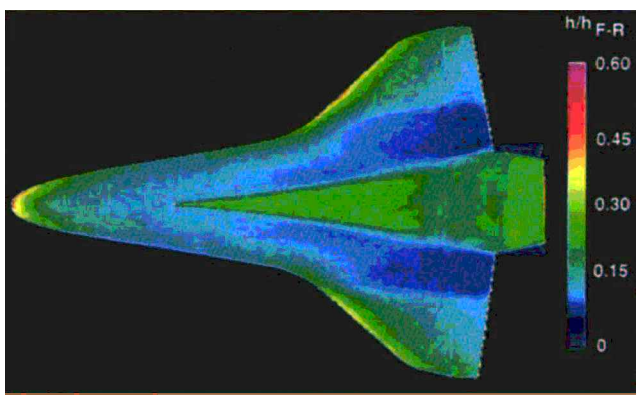

0.0075-in. roughness element and $Re_\infty = 2.2 \times 10^6$/ft

Fig. 7 Effect of trip height on transition at location G showing the effective freestream unit Reynolds number ($M_\infty = 6$, $\alpha = 40$ deg).

Figure 6 presents the centerline heating results for three different cases (0.0025-, 0.0050-, and 0.0075-in. trips at location G) over a range of freestream unit Reynolds numbers. As stated previously, for each trip configuration the Reynolds number was incrementally varied to identify the incipient, critical, and effective values. As expected, as the trip height increased, a lower Reynolds number was required to promote transition. Figure 6a reveals that, for a 0.0025-in. trip at location G, the centerline remains laminar up to $Re = 3.1 \times 10^6$/ft, is highly transitional by $Re = 4.4 \times 10^6$/ft, and appears effective by approximately $Re = 4.8 \times 10^6$/ft. Figure 6b shows that, for a 0.0050-in. trip at location G, the centerline remains laminar up to $Re = 1.6 \times 10^6$/ft, is transitional by $Re = 1.9 \times 10^6$/ft, and appears effective by $Re = 2.4 \times 10^6$/ft. Figure 6c reveals that, for a 0.0075-in. trip at location G, the centerline remains laminar up to $Re = 1.1 \times 10^6$/ft, is transitional by $Re = 1.5 \times 10^6$/ft, and appears effective by $Re = 1.85 \times 10^6$/ft. The effective values were determined by comparing similar critical Reynolds numbers for the same trip height at different locations.

Figure 7 presents the phosphor thermography heating images for the runs most closely matched with the effective Reynolds number for the three cases presented in Fig. 6. The turbulent wedge appears to be fixed at the roughness location for these three cases, and the spreading angle of the turbulent wedge appears to be relatively consistent. Additional heating images corresponding to effective Reynolds numbers at locations E-CL and D, respectively, are presented in Figs. 8 and 9 for comparison. As the roughness location moves upstream, the turbulent wedge spreading angle appears to increase. This could be attributable to the strong lateral pressure gradient that exists in the nose region that produces the strong outflow evident near the nose in the oil-flow photograph shown in Fig. 10 (a typical Orbiter oil flow from the 20-Inch Mach 6 Tunnel at $\alpha = 40$ deg and $Re = 5.4 \times 10^6$/ft). In fact, at the most forward trip station (location A), inconsistent results were observed, evidently because of a sensitivity to extremely accurate placement of the roughness

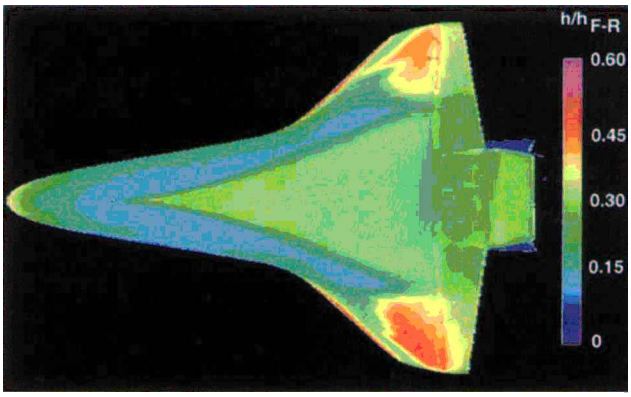

0.0025-in. roughness element and $Re_\infty = 5.8 \times 10^6$/ft

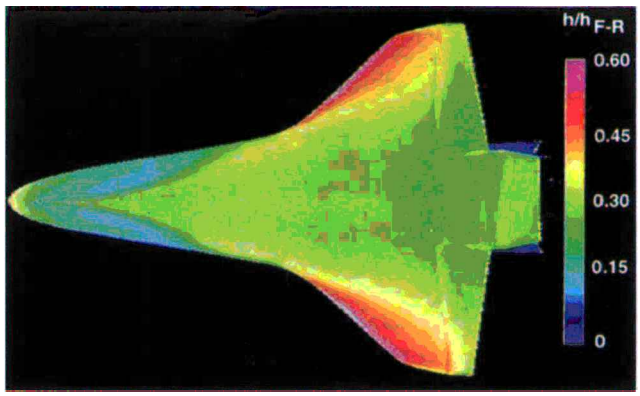

0.0025-in. roughness element and $Re_\infty = 5.4 \times 10^6$/ft

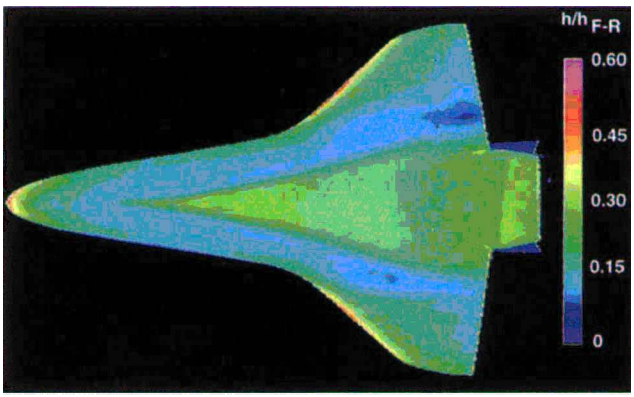

0.0050-in. roughness element and $Re_\infty = 3.1 \times 10^6$/ft

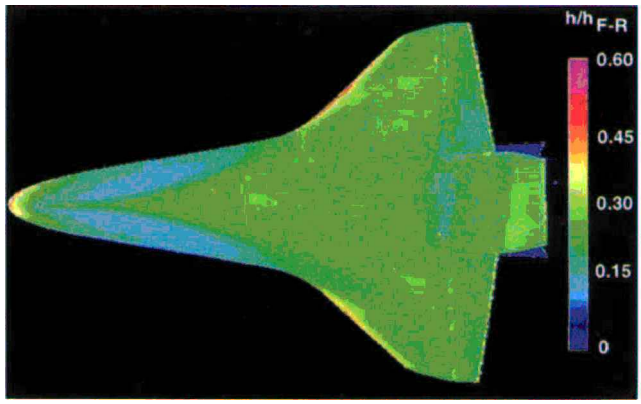

0.0050-in. roughness element and $Re_\infty = 2.7 \times 10^6$/ft

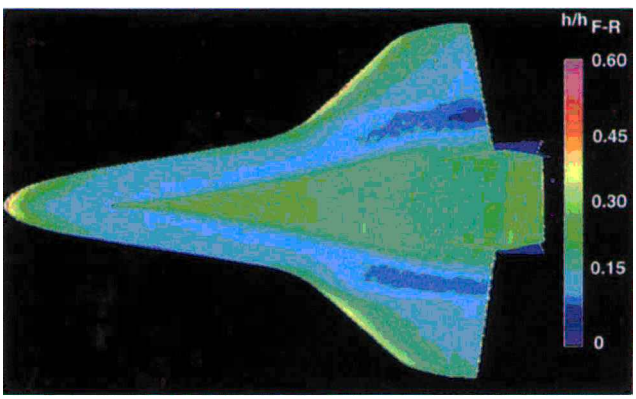

0.0075-in. roughness element and $Re_\infty = 2.2 \times 10^6$/ft

Fig. 8 Effect of trip height on transition at location E-CL showing the effective freestream unit Reynolds number ($M_\infty = 6$, $\alpha = 40$ deg).

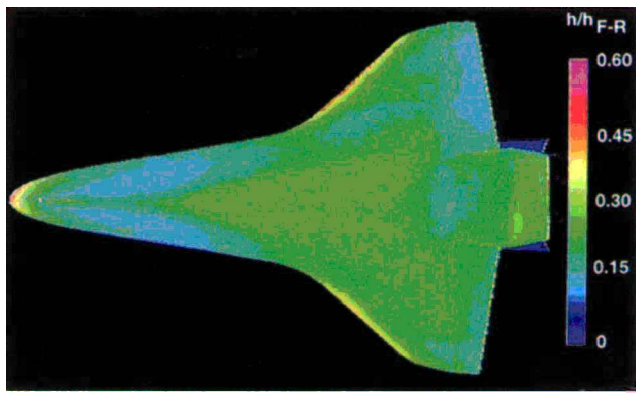

0.0075-in. roughness element and $Re_\infty = 1.8 \times 10^6$/ft

Fig. 9 Effect of trip height on transition at location D showing the effective freestream unit Reynolds number ($M_\infty = 6$, $\alpha = 40$ deg).

elements on the windward centerline. It is hypothesized that the inconsistent results were again due to the strong lateral pressure gradient near the nose, coupled with slightly inaccurate placement of the trips, producing strongly asymmetric disturbances behind the trip. Because of the inconsistent results at location A, these results are not included in this data set.

Roughness Correlation

A shuttle-derived, roughness-induced transition correlation for the present series of tests in the LaRC 20-Inch Mach 6 Tunnel is presented in Fig. 11. These results (see also Table 2 of Ref. 9) are presented as Re_θ/M_e vs k/δ and include the incipient and effective centerline results. The trip configuration numbers, i.e., G1, where G is the location and 1 denotes the height as 0.0025-in., are included. Collectively, these results for a wide range of trip locations and sizes produced a well-behaved trend in terms of Re_θ/M_e vs k/δ. To the left side of the incipient curve, the model remained laminar, whereas on the right side of the effective curve, the turbulent wedge was fixed at the roughness element. The relationship $Re_\theta/M_e = C(k/\delta)^{-1}$, where $C = 21$ for incipient and 30 for effective, appears to represent the data. The data presented in this correlation plot were very repeatable, including trends from two identical (primary and backup) models.

Turbulent Spreading Angle

Figure 12 presents a comparison of the turbulent wedge spreading half-angles for the present data set and the data presented by Fischer[15] for a variety of Mach numbers and configurations. The present spreading angles were determined from the effective images at a point $\Delta x/L = 0.2$ behind the trip. Spreading of the streamlines has not been accounted for. However, along the centerline, streamline spreading should be at a minimum. The present higher-edge Mach number data (farther aft on the model) lie within the scatter of Fischer's data and the lower-edge Mach number data (closer to the nose and, thus, more streamline spreading) slightly above Fischer's data.

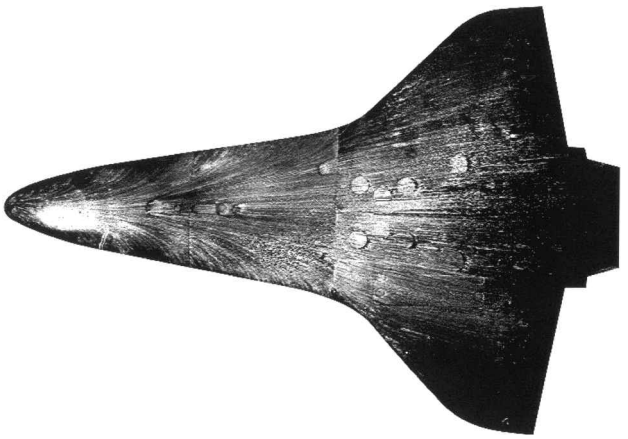

Fig. 10 Representative oil-flow result showing spreading of windward surface streamlines ($M_\infty = 6$, $\alpha = 40$ deg, $Re_\infty = 5.4 \times 10^6$/ft).

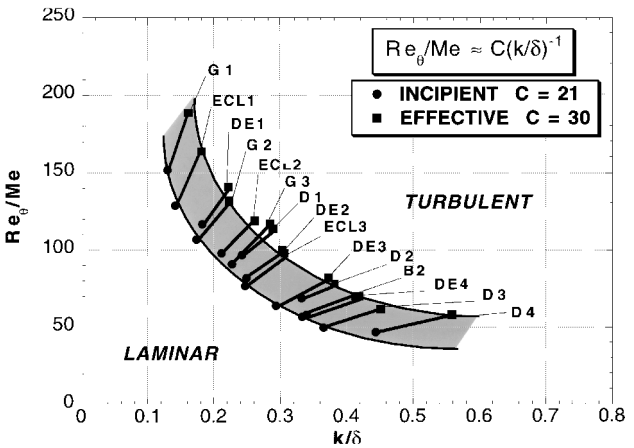

Fig. 11 Shuttle Orbiter centerline roughness transition correlation for LaRC 20-Inch Mach 6 Tunnel ($\alpha = 40$ deg).

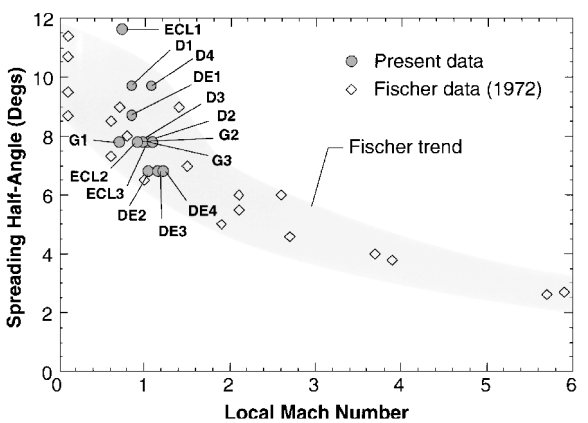

Fig. 12 Turbulent spreading half-angle results for centerline data ($\alpha = 40$ deg).

Off-Centerline Results

A few off-centerline effective images have been included for comparison. Figure 13 presents the heating image for the case in which a 0.0075-in. trip was placed just outboard of location C at $Re = 3.16 \times 10^6$/ft. Note that, for this off-center location, the turbulent wedge that is produced now affects only one side of the vehicle. This asymmetric condition has been hypothesized to promote the anomalous yawing moments measured during several Shuttle missions. Figure 14 presents two images in which multiple trips were placed on the windward surface (a 0.0025-in. trip is placed at location C, and a 0.0050-in. trip is placed at location K) for $Re = 3.14 \times 10^6$/ft and 4.34×10^6/ft, respectively. In Fig. 14a, the Reynolds number is such that transition is forced to the location-K

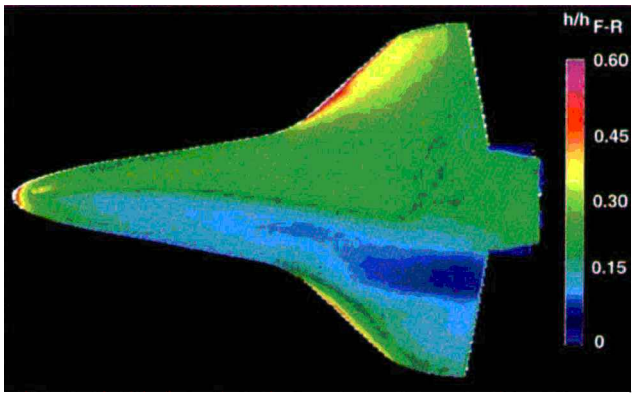

Fig. 13 Windward heating image for 0.0075-in., off-centerline trip outboard of location C at $Re_\infty = 3.2 \times 10^6$/ft.

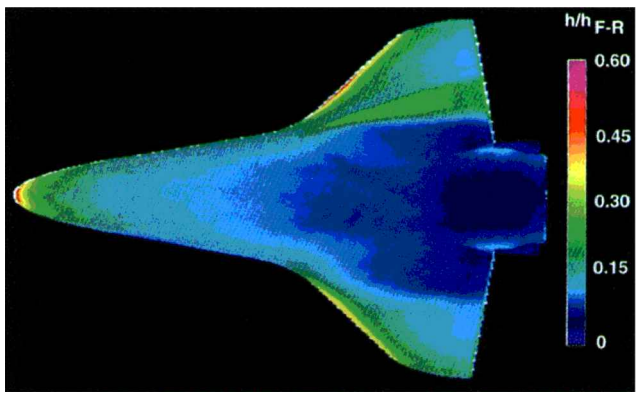

a) $Re_\infty = 3.1 \times 10^6$/ft

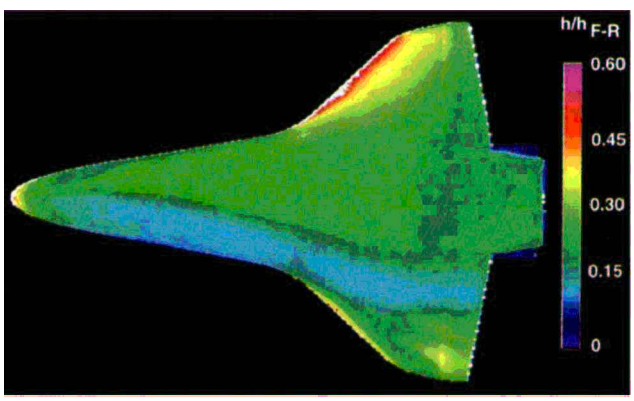

b) $Re_\infty = 4.3 \times 10^6$/ft

Fig. 14 Effect of freestream unit Reynolds number for double-trip case of 0.0025-in. trip at location C and 0.0050-in. trip at location K.

trip, but as the Reynolds number increases slightly (Fig. 14b), the turbulent wedge jumps to location C. These images provide an example of how separate roughness elements can give the impression of turbulence flashing forward on Orbiter, as had been observed in the flight data.

Concluding Remarks

An investigation into the effect of isolated roughness elements on hypersonic boundary-layer transition on the Shuttle Orbiter has been performed in the NASA LaRC 20-Inch Mach 6 Tunnel over a range of freestream unit Reynolds numbers. Phosphor thermography was used to provide global heating images of the windward surface. The size and location of isolated roughness elements were varied to systematically examine the response of the boundary layer, i.e., laminar, transitional, or turbulent, as inferred from the heating images. Computational predictions were performed to provide heating

levels for comparison to the experimental data and to provide flowfield parameters used for boundary-layer transition correlations.

A roughness-transition correlation, using the transition parameters Re_θ/M_e and the disturbance parameter k/δ, was well behaved along the centerline for $\alpha = 40$ deg. A functional relationship between these two parameters consistently predicted both the onset of transition and fully turbulent flow at the roughness element. These trends may have significance for similar re-entry vehicles.

The high spatial resolution provided by the phosphor technique clearly identifies the turbulent wedge that can be generated by an isolated roughness element, such as a protruding gap filler in flight. The spreading angles associated with the turbulent disturbances were measured from the images and compared well to previous ground-based data. The off-centerline results, although not included in the correlation, illustrate the potential for turbulence to be isolated to one side of the flight vehicle, which could explain the increased yawing-moment anomalies experienced by the Orbiter in flight.

References

[1]Bertin, J. J., Stetson, K. F., Bouslog, S. A., and Caram, J. M., "Effect of Isolated Roughness Elements on Boundary-Layer Transition for Shuttle Orbiter," AIAA Paper 96-1906, June 1996.

[2]Miller, C. G., "Langley Hypersonic Aerodynamic/Aerothermodynamic Testing Capabilities—Present and Future," AIAA Paper 90-1376, June 1990.

[3]Buck, G. M., "Automated Thermal Mapping Techniques Using Chromatic Image Analysis," NASA TM-101554, 1989.

[4]Buck, G. M., "Surface Temperature/Heat Transfer Measurement Using a Quantitative Phosphor Thermography System," AIAA Paper 91-0064, Jan. 1991.

[5]Merski, N. R., "A Relative-Intensity Two-Color Phosphor Thermography System," NASA TM-104123, 1991.

[6]Micol, J. R., "Aerothermodynamic Measurement and Prediction for a Modified Orbiter at Mach 6 and 10 in Air," *Journal of Spacecraft and Rockets*, Vol. 32, No. 5, 1995, pp. 737–748; also AIAA Paper 91-1436, June 1991.

[7]Buck, G. M., and Vasquez, P., "An Investment Ceramic Slip-Casting Technique for Net-Form, Precision, Detailed Casting of Ceramic Models," U.S. Patent 5,266,252, Nov. 1993.

[8]Bouslog, S. A., An, M. A., and Derry, S. A., "Orbiter Windward-Surface Boundary-Layer Transition Flight Data," *Orbiter Experiments (OEX) Aerothermodynamics Symposium*, NASA CP-3248, 1995, pp. 703–739.

[9]Berry, S. A., Bouslog, S. A., Brauckmann, G. J., and Caram, J. M., "Boundary Layer Transition Due to Isolated Roughness: Shuttle Results from the LaRC 20-Inch Mach 6 Tunnel," AIAA Paper 97-0273, Jan. 1997.

[10]Fay, J. A., and Ridell, F. R., "Theory of Stagnation Point Heat Transfer in Dissociated Air," *Journal of the Aeronautical Sciences*, Vol. 25, No. 2, 1958, pp. 73–85.

[11]An, M. Y., Wang, K. C., and Tam, L. T., "Computation of Inviscid Flowfield Around 3-D Aerospace Vehicles and Comparison with Experimental and Flight Data," AIAA Paper 93-0885, Jan. 1993.

[12]Wang, K. C., "An Axisymmetric Analog Two-Layer Convective Heating Procedure with Application to the Evaluation of Space Shuttle Orbiter Wing Leading Edge and Windward Surface Heating," NASA CR-188343, 1994.

[13]Murray, A. L., "Further Enhancements of the BLIMP Computer Code and User's Guide," AFWAL-TR- 3010, Wright–Patterson AFB, OH, June 1988.

[14]Bouslog, S. A., Bertin, J. J., Berry, S. A., and Caram, J. M., "Isolated Roughness Induced Boundary-Layer Transition: Shuttle Orbiter Ground Tests and Flight Experience," AIAA Paper 97-0274, Jan. 1997.

[15]Fischer, M. C., "Spreading of a Turbulent Disturbance," *AIAA Journal*, Vol. 10, No. 7, 1972, pp. 957–959.

T. C. Lin
Associate Editor

Color reproduction courtesy of NASA Langley Research Center